

# Right Lateral Shear and Rotation in the Northeast of the Arabian-Iranian Collision Zone

Arash Barjasteh \*

Deputy for Dam and Power Plant Development, Khuzestan Water and Power Authority, Ahvaz, Iran

 Arash Barjasteh: <https://orcid.org/0000-0001-9465-1848>

**ABSTRACT:** Accommodation of continental convergence by crustal thickening and lateral transport is mainly featured as strike-slip faulting along the trends roughly orthogonal to the orientation of plate convergence. This style of faulting will affect seismicity of the involving areas which can be proved in low seismic zones by determining regional stress pattern using numerical methods. Accordingly, the stress distribution and deformation pattern of the South Sanandaj-Sirjan zone in the northeastern part of the Iranian-Arabian collision zone is investigated here using a three dimensional mechanical model. The modeled area is bounded between the Zagros thrust fault on the west and Dehshir-Baft fault in the east. The model is composed of three layers: the upper two layers represent the upper brittle and lower ductile crust of the collided continent and the lowest layer represents the lithospheric mantle. The upper crust behaves as an elastic material while the lower crust is considered as a non-Newtonian viscous fluid layer. The lithospheric mantle is taken as a low-viscosity material which is not allowed to move in any direction relative to the overlying layers. The Zagros thrust fault was treated with two different dip values saying 90° and 45° but Dehshir-Baft fault was modeled as a vertical fault and allowed to have a dextral movement regarding to the existing evidence. The driving mechanism applied to the western side of the model was chosen considering two different approaches including a kinematic approach (the Arabian-Eurasian convergence velocity; 35 mm/yr) and a dynamic approach (an external boundary force equal to 3.55E+17 N). The resulted stress field indicates an orogen-parallel component of right lateral shear along the Zagros fault implying a rotational deformation pattern within the modeled region that suggests a stress partitioning in the study area. The pattern also indicates a stress accumulation towards the south which could be a reason for the regional seismic quiescence between the two seismic Zagros thrust and Dehshir-Baft faults. Based on the present modeling results, it seems that high stress localization on the boundary faults can be a support of block structure approach or quasi-rigid blocks deformation within the study area. The resultant patterns of stress and displacement fields are generally totally comparable with plate boundary shear zones and have been proven by field data.

**KEY WORDS:** Zagros thrust fault, Sanandaj-Sirjan belt, numerical modeling, shear zone, Eghlid-Deh Bid.

## 0 INTRODUCTION

Surface deformation associated with faulting can be modeled by assuming a layered rheology (Sargent, 2004; Bonini et al., 2003; Sobouti and Arkani-Hamed, 1996; Jackson et al., 1995) with an elastic layer overlying one or more viscous or visco-elastic layers. The difference in the proposed rheology which results in a viscosity contrast can affect the kinematics and dynamics of the shear zones accompanied with oblique convergent plate boundaries such as the Iranian-Arabian collision zone. Here we model Eghlid-Deh Bid area in the northeastern part of the

Zagros fold-thrust belt (ZFTB) with a numerical code and describe stress distribution across it regarding its bounding fault systems. In spite of previous models (for example Jackson et al., 1995) we consider the Sanandaj-Sirjan metamorphic belt (SSB) as a separate block intervening the Zagros belt and Central Iran by including its bounding faults as deep seated discontinuities in the model. It was predicted that an asymmetric stress pattern and surface velocity field would be observed. This might cause strain partitioning in the area behind the line of collision. The importance of the selected area is that it includes the SSB (Stocklin, 1968) with a complex structure which is apparently an aseismic zone (Ambraseys and Jackson, 1998; Ambraseys and Melville, 1982). The tectonic activity of Zagros and Central Iran (e.g., Jackson and McKenzie, 1984) is a combination of thrusting and folding within the former, while strike-slip faulting dominates in the latter. However, the interaction between the above mentioned mechanisms have to be

\*Corresponding author: barjasteh@hotmail.com

© China University of Geosciences and Springer-Verlag GmbH Germany, Part of Springer Nature 2018

Manuscript received January 20, 2017.

Manuscript accepted May 15, 2017.

investigated in the intervening region, the Sanandaj-Sirjan belt. Also, it is expected that motion along the Zagros thrust fault is taken up by differential motion at the borders of the SSB. This can produce a rotational stress pattern that causes rotation and deflection of the local structures. The final modeled pattern of stress and displacement could be used to predict seismic behavior of the bounding faults tectonic activity inside the study area. A few studies have been carried out on the dynamics of the Iranian-Arabian collision zone (IACZ) using numerical models. Among those works, it is the pioneer article of Bird (1978) that discussed its deformation along a vertical  $X$ - $Z$  plane and explained mainly its responsible driven forces. Sobouti and Arkani-Hamed (1996) described a two dimensional finite element model based on a mathematical formulation established by England and McKenzie (1982), which was applied to investigate deformational history of the Iranian Plateau in the  $X$ - $Y$  plane. The main difference in approach of the two papers are the geometrical boundaries of the studied area which, in the former, run from the Red Sea Ridge zone to the Zagros thrust line (ZTL) and in the latter from the ZTL to the eastern boundary of the Iranian Plate with Afghanistan Mountain ranges. Some more recent studies apply 2D and 3D finite element models to evaluate different aspects of crustal movements and shortening along and across the IACZ (e.g., Vernant and Chéry, 2006a, b; Masson et al., 2005; McQuarrie, 2004; McQuarrie et al., 2003).

However, 2D models are affected by some limitations such as plane strain assumption inherited in it (Seyferth and Henk, 2004). In this paper, a 3D finite element model code, TECTON 2.3 (Melosh and Williams, 1989; Melosh and Raefsky, 1980) was applied to simulate the deformation pattern

of the study area (Fig. 1) due to main regional fault geometries (Fig. 2), to show how these can influence the stress pattern and style of deformation in the study area.

## 1 NUMERICAL METHOD, GEOMETRY AND BOUNDARY CONDITIONS

The main purpose of this paper is to model deformation pattern of the southern part of the Sanandaj-Sirjan belt (the South Sanandaj-Sirjan) bounded by the Zagros thrust and Dehshir-Baft faults in the northeast of the Arabian-Iranian collision zone. This approach is basically suitable for assessing the role of the bounding faults regarding block structure dynamics (Keilis-Borok et al., 1997). The modeled area is almost located between 30°N–32°N and 52°E–54°E that covers Eqhlid-Deh Bid area (EDA). The selected area for modeling defines an upside down triangle (Fig. 1) of which each edge is coincident with a clear structural element or a tectonic lineament. The boundaries of the model are primarily based on the previous model works (Vernant and Chéry, 2006a; Sobouti and Arkani-Hamed, 1996; Bird, 1978). This selection took into consideration the main structural fracture trends recognized for the Iranian Plateau (Fig. 2). The western edge (trending NW-SE) represents Zagros thrust fault line (ZTL) and the eastern edge (trending nearly N-S) coincides with Dehshir-Baft fault (DBF). This fault is very important as a prevailing structure with total length of about 380 km as the boundary between the SSB and the Central Iran (CI). It has displaced right-laterally major structural trends of the SSB (Meyer et al., 2006; Berberian and Berberian, 1981). The third edge is defined by a nearly E-W trending lineament that is clearly detectable in most of the Central and Eastern Iran (McQuillan, 1991; Kronberg, 1983). This assumption is reinforced

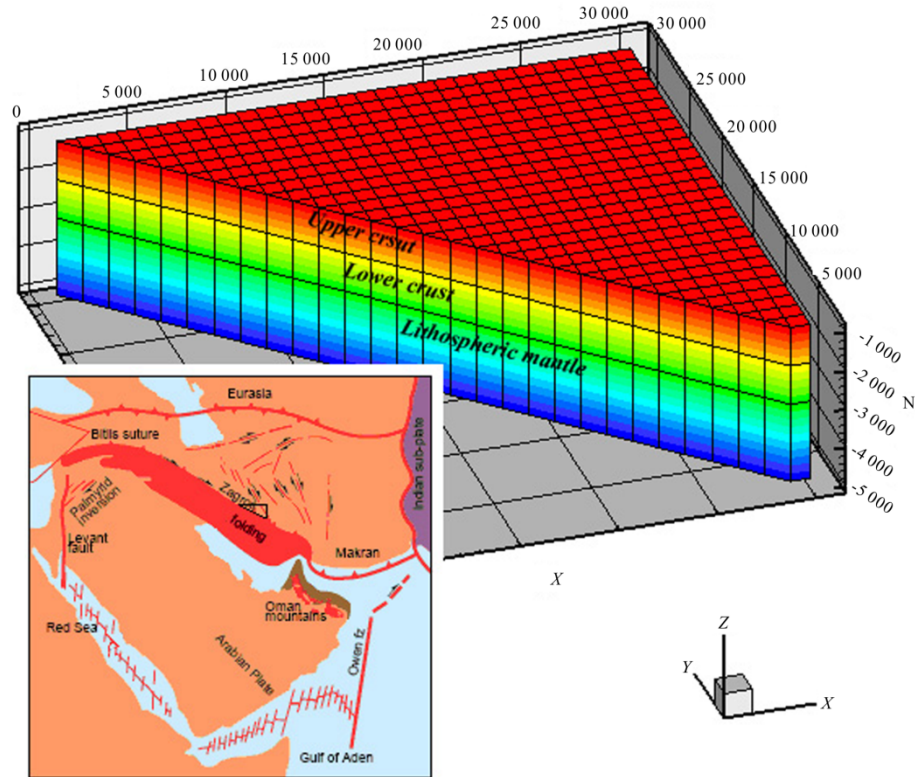


**Figure 1.** General grid mesh of the study area and its location within the Iranian Plateau.

regarding to occurrence of some nearly E-W trending folds along this boundary (Houshmandzadeh et al., 1975) and faulting (Sarkarinejad and Ghanbarian, 2014; Shafiei et al., 2011). GPS measurements below the mentioned trend and above it indicated a westward movement north of it and an eastward movement south of it (Walpersdorf et al., 2006). Additionally, this E-W trending boundary was selected for the simplicity of model geometry.

In this modeling, a 3D finite element code, TECTON 2.3 (Melosh and Williams, 1989; Melosh and Raefsky, 1980) with two kinematic and dynamics approaches was used to analyze stress and displacement patterns in the area and their downward variation due to the extent of faulting in depth. Besides,

the study area (that is the South SSB) was considered as a separate block distinguished from its surrounding zones by deep seated faults i.e., ZTL and DBF. Such an approach was applied somehow in the previous works (Reilinger et al., 2006; Vernant and Chéry, 2006b). The outputs were then reformatting, restructured and transferred to Tecplot 10 software (Tecplot Inc., 2005) where all the final figures were displayed and edited.

The grid is a 3D mesh composed of 1 856 elements (Fig. 3) with a total area of about 4 000 km<sup>2</sup> (nearly 200 km × 200 km sides). The first row of the western side of the grid includes triangular elements while the rest of it is composed of rectangular ones. The model did not consider thermal changes due to

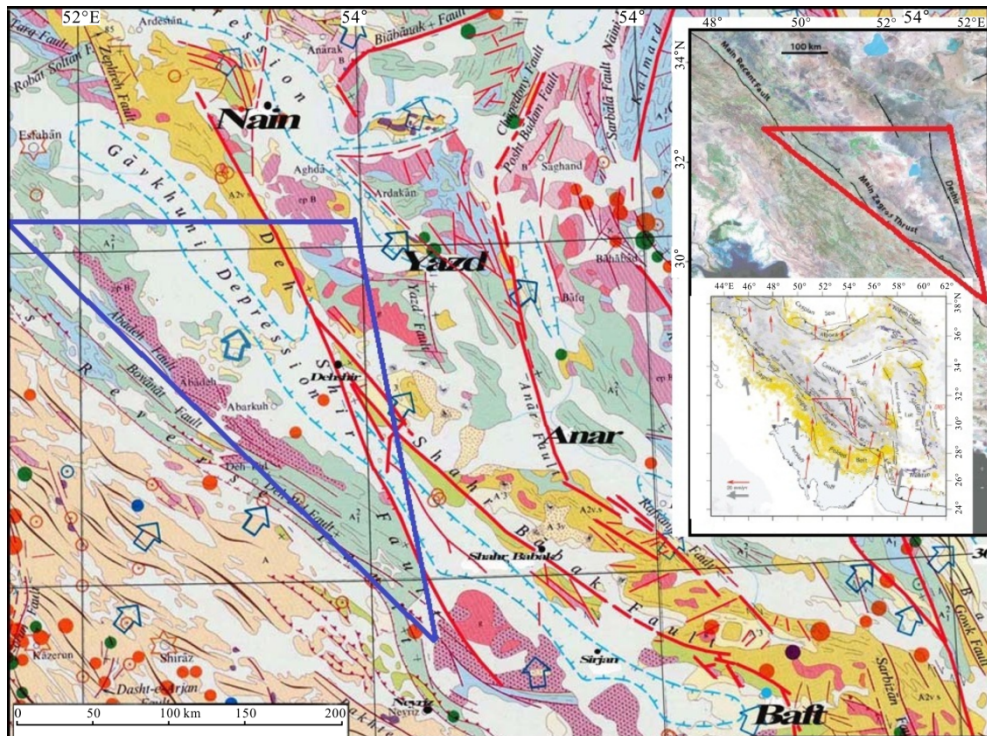


**Figure 2.** Geological boundaries of the study area and its location within the Iranian Plateau (modified after NIOC, 1975 and Walker and Jackson, 2004).

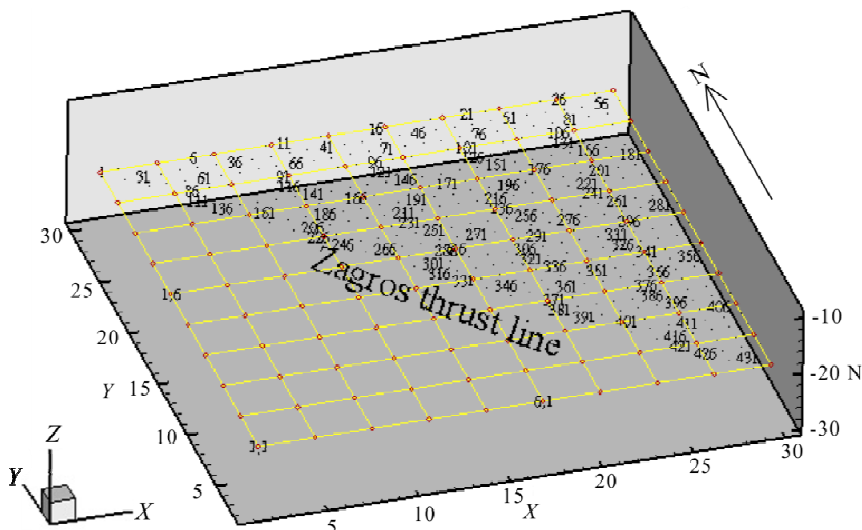


**Figure 3.** Simplified mesh plot of the study area showing order of nodes numbering.

geothermal gradient or any temperature variation resulting by mechanical changes. The lithosphere is considered to consist of upper crust and lower crust overlying asthenosphere. A total thickness of 100 km is given to the domain comprising of three layers. The upper two layers are competent and represent the upper brittle and lower ductile crust of the collided continent with a thickness of 20 and 40 km, respectively, and the lowest layer represents lithospheric mantle. The upper crust behaves as an elastic material while the lower crust is considered as a non-Newtonian viscous fluid layer with varying power law exponents ( $n=1$  in kinematic approach and  $n=3, 5, 7$  in dynamic approach). The lithospheric mantle is taken as a low-viscosity material and is not allowed to move in any direction relative to the overlying layers. Here, a no-slip boundary condition along its base is applied (Sokoutis et al., 2000). For this reason, the base of it has been fixed in all directions (zero boundary condition in  $X$ ,  $Y$ , and  $Z$ ) by applying a fixed displacement criterion as maintained in the code. The ZTL is the only advancing boundary which defines the location where external boundary forces act on the model. The boundary conditions applied to the sides of the model are in terms of velocity and expected movement directions of major fault trends as mentioned above (Sarkarinejad and Barjasteh, 2010, 2008). On the eastern boundary (DBF) we let the boundary to displace in  $Y$ -direction without any specified amount of velocity on it but corresponding to the resolution of the convergence velocity. The third side is taken to move freely in  $X$ -direction regarding the behavior of similar fault trends in the Iranian Plateau. The apexes of the triangular model were pinned for all directions, as well. A time interval of 1.5 Ma (Allen et al., 2004; Boulin, 1991) is selected to investigate deformation pattern of the study area in a kinematic approach (Sargent, 2004) with a total time of 15 Ma. The summary of the input variables are shown in Table 1. The main material properties of elements are: Young's modulus ( $E$ ), Poisson's ratio, density and viscosity coefficient. The above list is basically for visco-elastic elements. If any element supports plastic yield, some additional properties are included in the code as follows: angle of internal friction ( $\phi$ ), cohesion or yield stress ( $C$ ), fluidity for visco-plastic yield ( $\gamma$ ) and a strain hardening parameter.

In this paper a Drucker-Prager formulation will be used for calculations. The lithosphere is considered to consist of

**Table 1** Summary of physical parameters used in the mechanical modeling

| Name                  | Symbol   | Unit                             | Value  |
|-----------------------|----------|----------------------------------|--|
| Young's modulus       | $E$      | Pa                               | 1.00E+11   |
| Poisson's ratio       | $\nu$    |                                  | 0.25   |
| Density               | $\rho$   | gcm <sup>-3</sup>                | 2.80E+3 (upper crust)<br>2.70E+3 (lower crust)<br>3.00E+3 (upper mantle) |
| Viscosity coefficient | $\eta$   | Pa·s                             | 1.00E+11<br>1.0 (lower crust)  |
| Power law             |          |                                  |  |
| Cohesion              | $C$      | Pa                               | 1.00E+7  |
| Friction angle        | $\phi$   | °                                | 30   |
| Fluidity parameter    | $\gamma$ | Pa <sup>-1</sup> s <sup>-1</sup> | 1.00E-5  |

upper crust and lower crust overlying asthenosphere. A total thickness of 100 km is given to the domain comprising three layers. The upper two layers are competent and represent the upper brittle and lower ductile crust of the collided continent with a thickness of 20 and 40 km, respectively, and the lowest layer represents lithospheric mantle. The upper crust behaves as an elastic material while the lower crust is considered as a non-Newtonian viscous fluid layer with a low power law exponent ( $n=1.0$ ). The lithospheric mantle is taken as a low-viscosity material and is not allowed to move in any direction relative to the overlying layers. Here, a no-slip boundary condition along its base is applied (e.g., Sokoutis et al., 2000). For this reason, the base of the model has been fixed in all directions (zero boundary condition in  $X$ ,  $Y$ , and  $Z$ ) by applying a fixed displacement criterion as maintained in the code. The boundary conditions applied to the sides of the model are velocity and expected movement directions of major fault trends. The ZTL is the only advancing boundary which defines the location where external boundary forces act on the model. Following Sobouti and Arkani-Hamed (1996), the Arabian convergence velocity (35 mm·yr<sup>-1</sup>) toward Eurasia as noted by Kreemer et al. (2003) and DeMets et al. (1990) is applied to the western side of the model (ZTL) in  $Y$ -direction as the driving velocity.

## 2 RESULTS OF THE MODEL

The results of the modeling experiment are given in two parts. First, the characteristic features of the modeled stress field for different components are presented. Second, the resulted displacement vectors along and across the domain boundaries are illustrated and interpreted. The model analyzed stress and displacement pattern in  $XY$ ,  $XZ$  and  $YZ$  sections to find their downward variation due to the extent of faulting in depth and density contrast. Also it investigated the role of change in fault dip to see how it might influence deformation pattern. The boundary conditions applied to the sides of the model are velocity and expected movement directions of major fault trends. The elements on the right side of the eastern boundary (DBF) were fixed. The third side is taken as a vertical fault plane with two different boundary conditions.

### 2.1 Stress Field Pattern

Figures 4a–4d show different components of the stress field resulting from our modeling. The amount of different stress components are shown as contours whereas the vectors superimposed on the diagrams indicated direction of  $S_{XY}$  vs.  $S_{YZ}$  values. The overall pattern of the stress variation is nearly similar for the normal components of the stress i.e.,  $S_{XX}$ ,  $S_{YY}$  and  $S_{ZZ}$  (Figs. 4a, 4b and 4d).

Their pattern is triangular and is very consistent with the shape of domain boundaries but its elongation is parallel to the  $Y$ -axis for  $S_{XX}$  and to the  $X$ -axis for  $S_{YY}$ . Besides, the direction of the stress increase is towards E and N for  $S_{XX}$  and  $S_{YY}$  components, respectively. The lower left sides of the plots have been automatically simulated and extrapolated by Tecplot 10. The stress field pattern of the shear component ( $S_{XY}$ ) is of course different from the normal ones and is almost symmetric about the ZFTB (Fig. 8c). It is changing in a direction parallel

to the plate convergence vector that is perpendicular to the plate boundary (the western side of the model i.e., the ZFTB). Generally, the stress pattern demonstrates an indication of asymmetry in the study area that could imply a strain partitioning within the area (Sarkarnejad, 2005, 2003; Mohajjal et al., 2003; Mohajjal and Fergusson, 2000). A similar pattern can be produced within shear zones dominating by right lateral strike slip faulting (Walker and Jackson, 2004; McKenzie and Jackson, 1983) with the differential movement of the bounding faults (Bonini et al., 2003).

## 2.2 Pattern of Displacement Vectors

The pattern of displacement field is illustrated in two distinct plots to better see its variation across the modeled area (Fig. 5). Its 2D contour plots are shown in Figs. 5a and 5b and its 3D contour diagram overlaid by a vector plot are demonstrated in Figs. 5c and 5d. The displacement pattern in  $X$ -direction is shown in the upper and its pattern in  $Y$ -direction is shown in the lower figures, respectively. The maximum amount of  $X$ -displacement is along the upper boundary of the model that is along the inferred E-W lineament trend.

On the other hand, the main zone of  $Y$ -displacement is where the western and eastern boundaries converge. This result is in very agreement with some recent observations of right

lateral strike-slip movement along the DBF (Meyer et al., 2006). The contours of  $Y$ -displacement show a necking along the trend of the ZTL in the western side of the figure with a southward increase. The contour graphs on the right side of the Fig. 5, present synoptic plots of the convergence direction and the modeled displacement field. The pattern of the displacement predicts a northward movement which rotates along the upper boundary. This shape might be partly affected by the geometry and initial conditions of the upper boundary (Soofi and King, 2002). However, such a change in the movement direction had been proved by GPS measurements (Walpersdorf et al., 2006) outside of the model limits that is westward and implies an eastward motion within the area (right pictures) to indicate the expected relative direction of movement along the model boundaries.

## 2.3 The Role of Dip Change on the Stress and Displacement Patterns

Of interest in this study was whether any changes in dip of the major boundary faults could have significant effect on the stress and displacement pattern. This was investigated by incorporating two different dips for the Zagros fault as the main advancing boundary into the model. The presence of faults within the lithosphere has been recognized as a factor

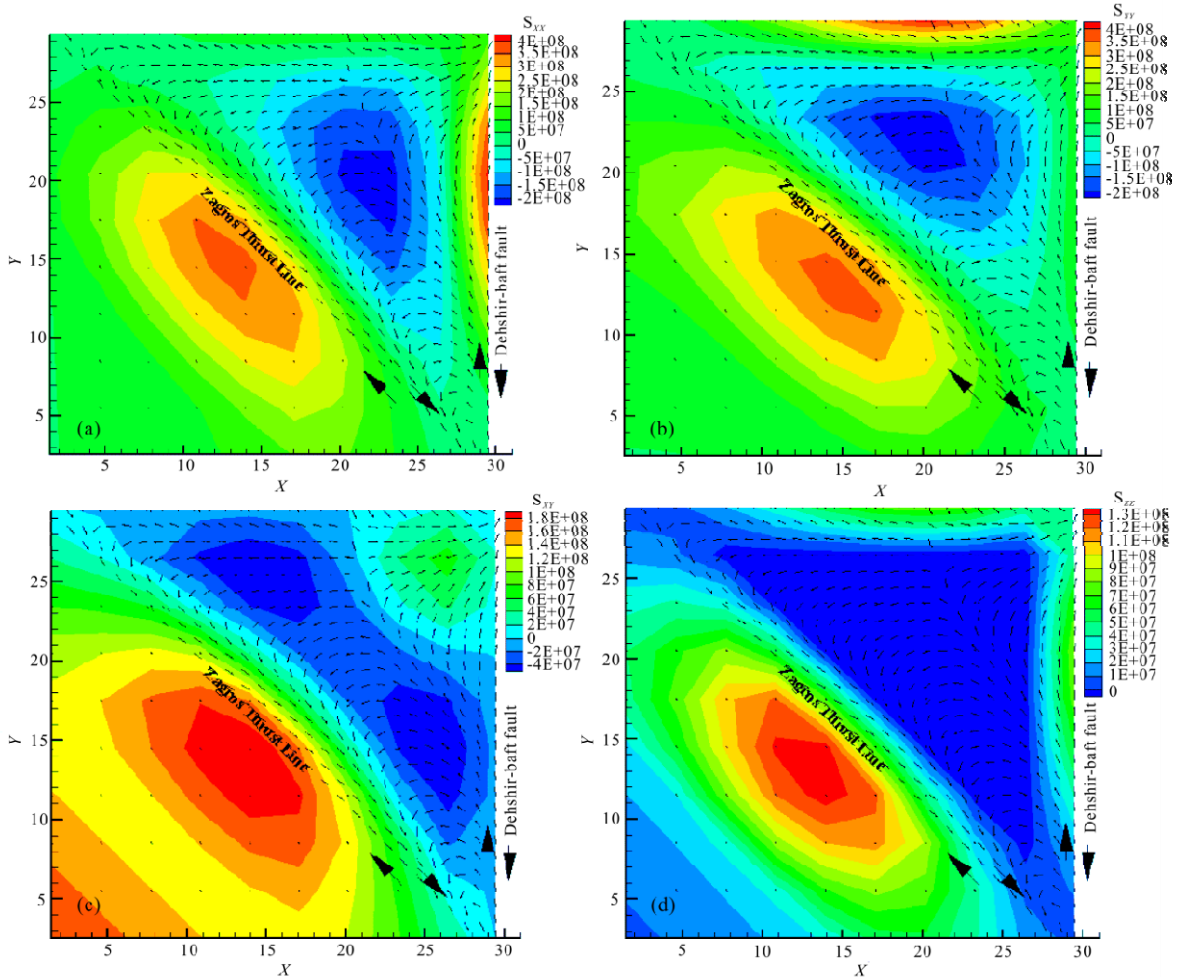


**Figure 4.** A synoptic two dimensional plot of the stress field patterns in the study area showing variation of  $S_{XX}$  (a),  $S_{YY}$  (b),  $S_{XY}$  (c) and  $S_Z$  (d) components in Pa.

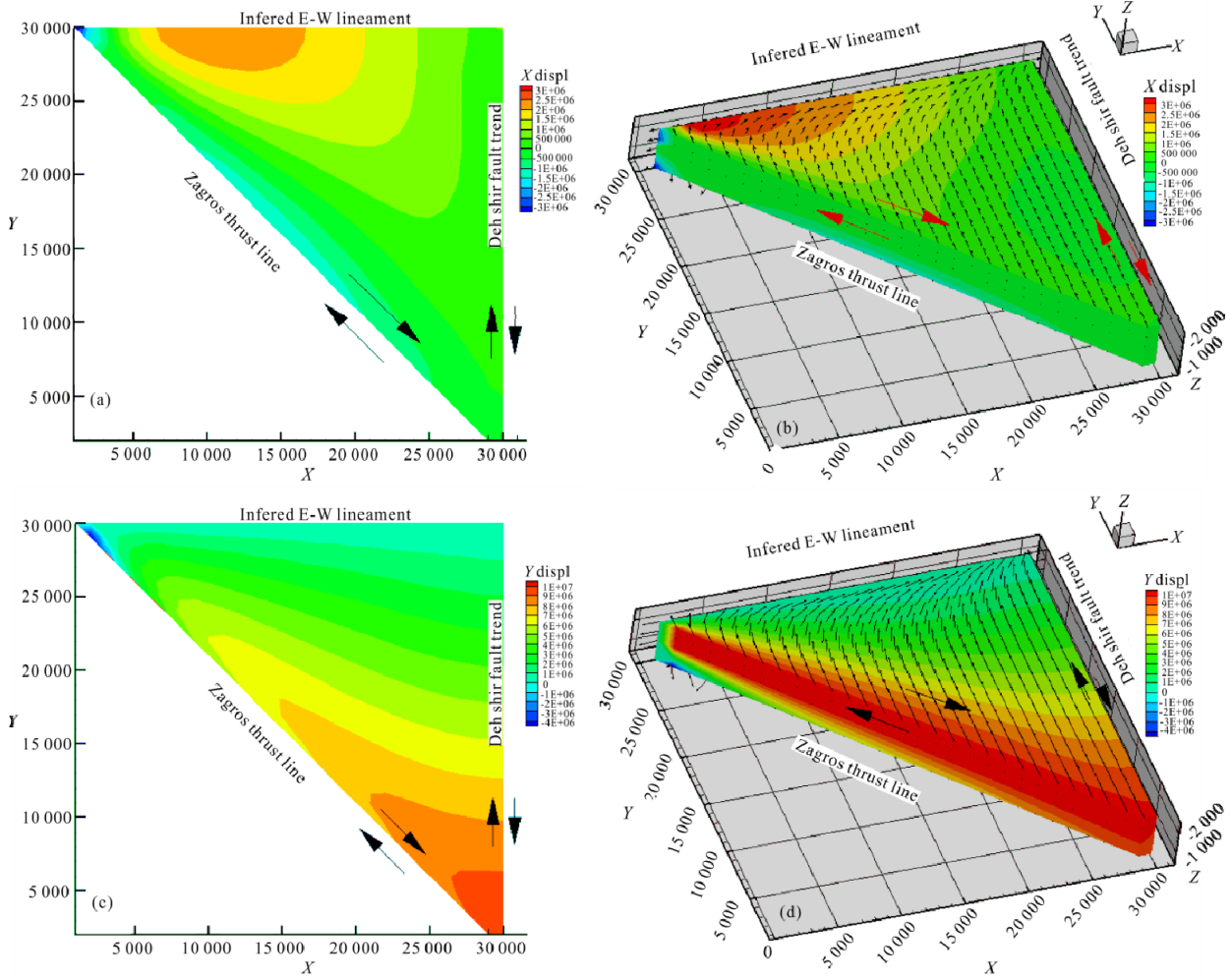


**Figure 5.** Contour plots of 2D ((a), (c)) and 3D ((b), (d)) of the displacement field components in the study area. A vector plot has been added to 3D illustrations.

influencing the behavior of the plate. It was mechanically shown that buckling stress, wavelength and the effective Young's modulus are dependent on fault depth and fault spacing (Wallace and Melosh, 1994). Thus, the present model tried to investigate the effect of faults in elastic part of the model that is down to the bottom of the lower crust.

To incorporate such a dip change, the grid thickness and length were fixed and a 45° dip plane was specified so that it passes through the opposing nodes of the corners of the cubed shaped elements. The contour plots of stress components due to change in dip of the Zagros fault, are presented in Fig. 6. In this figure, the left side block diagrams illustrate relevant fields for inclined Zagros fault (45°) while the right diagrams are due to a vertical one. Due to very small changes in the displacement pattern, the corresponding results for it are not presented here. Although, the effect of fault depth on deformation pattern was not investigated, it was incorporated in the model as the boundary faults were extended down to the bottom of the lower crust (Sarkarinejad and Barjasteh, 2010). The results show some differences for the two dip models. As is shown in Fig. 6, the stress patterns are more uniform for the case that the Zagros fault has 90° dip (Figs. 6b, 6d, 6f, 6h). However, the stress patterns show some localization along the boundaries for an inclined Zagros fault (Figs. 6a, 6c, 6e, 6g). Additionally, the

stress patterns in the former are more spread and lower in amount than that of the latter. However, such minor variations due to fault dip do not strongly affect either the stress pattern or the displacement field.

### 3 DISCUSSION

Regarding to the extent of boundary faults especially, the western side of the model as the advancing side, and to discuss the results of the present modeling, contour plots of the resultant stress field components are given in Fig. 7. The pattern is triangular and is very consistent with the shape of domain boundaries for the principal components (Figs. 7a, 7d). The simulation procedure has been merely based upon the original data within the domain boundaries and was extended to the left lower corner of the model area using Tecplot 10. The pattern of the shear component ( $S_{XY}$ ) is almost symmetric about the ZFTB (Fig. 7b) and shows a gradual decrease with increasing distance from it towards E. It is changing in a direction parallel to the plate convergence vector that is perpendicular to the plate boundary. The general direction of stress vectors are in good agreement with the expected movement direction along the boundaries, although some variation is visible especially along the northern margin. This was also checked for changing in the dip and movement manner of the bounding faults for

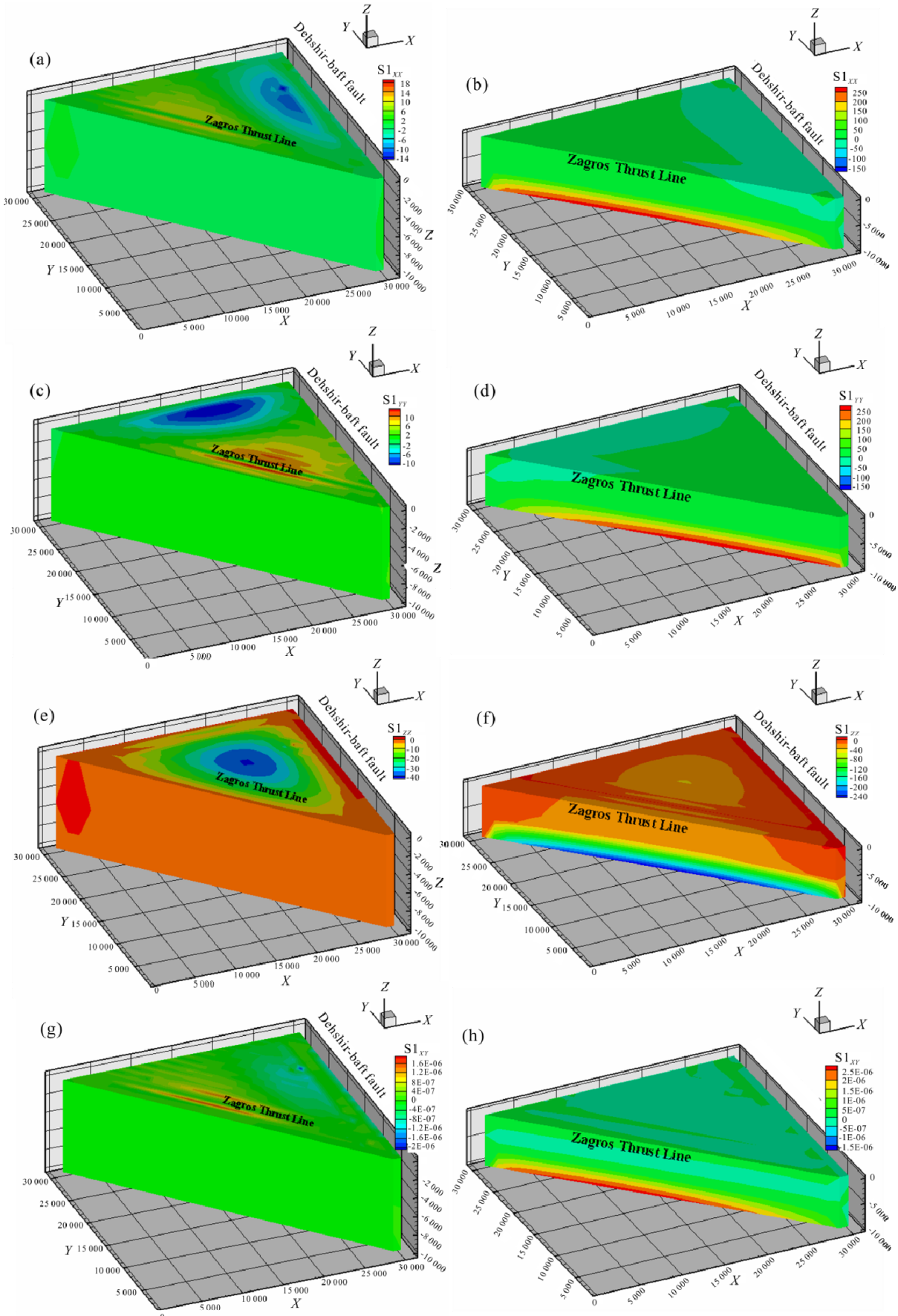
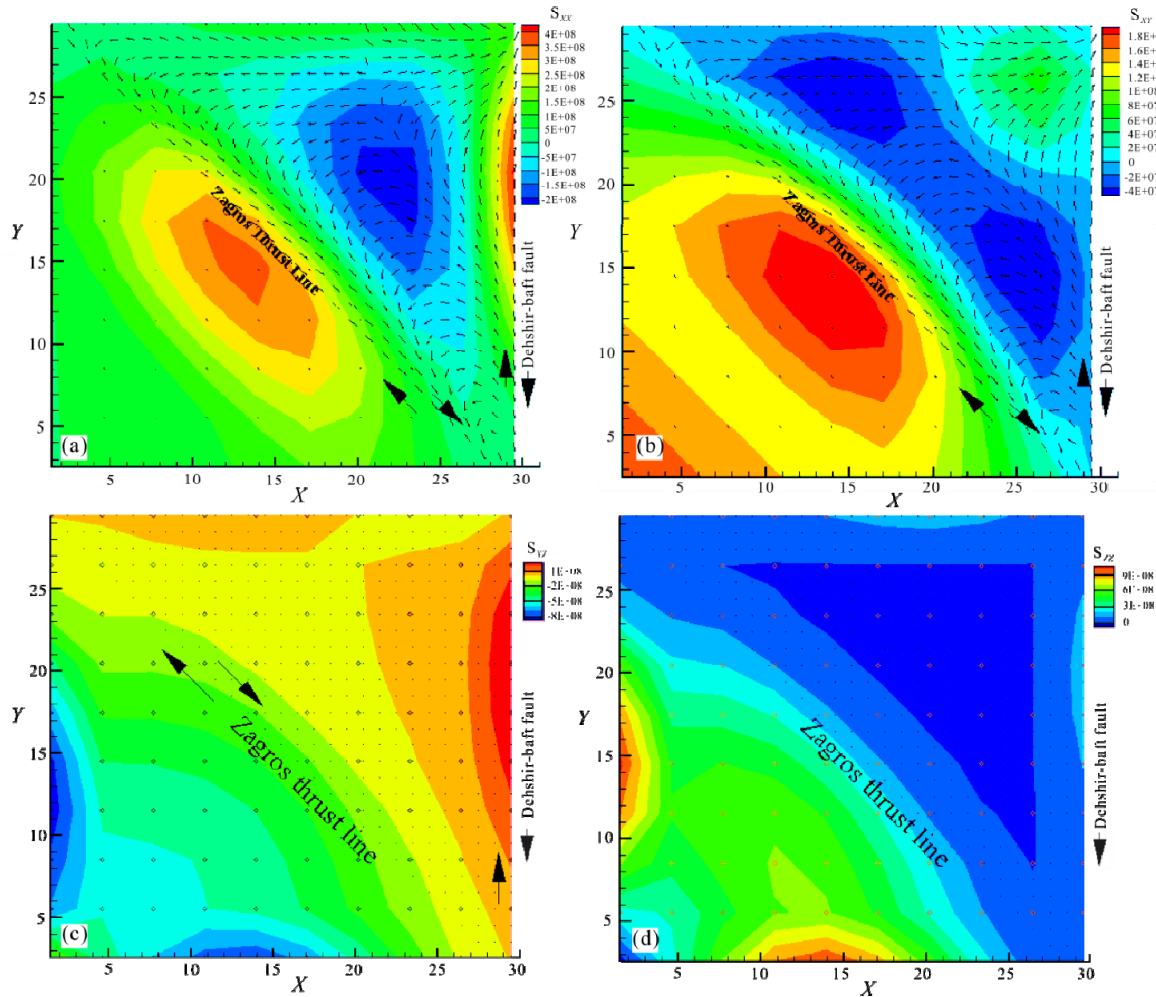


Figure 6. Block diagrams of contour plot of stress components (in Pa) due to change in dip of the Zagros fault (45 dip fault on the left and 90 dip fault on the right).



**Figure 7.** Stress field patterns of the study area showing variation of  $S_{XX}$  and  $S_{ZZ}$  ((a), (d)) and  $S_{XY}$  and  $S_{YZ}$  ((b), (c)) components (in Pa).

example, the Zagros thrust dip was considered oblique with an amount of 45°. In this case, the whole stress pattern changed especially along the upper margin of the model (Fig. 6). The displacement field in the study area demonstrated nearly similar patterns. The rotational manner of displacement field is easily visible at the southern corner where the western and eastern boundaries converge. The general northward pattern of the displacement and its subsequent rotation along the upper boundary might be affected by the geometry and initial conditions of the upper boundary (Soofi and King, 2002). The pattern is generally coincident with those predicted by previous works for the whole of the fold-thrust belt (e.g., Vernant and Chéry, 2006b; Sargent, 2004; Bonini et al., 2003; Sobouti and Arkani-Hamed, 1996; Jackson et al., 1995). The resulting stress and displacement patterns give an indication of asymmetry in the study area. This could imply a strain partitioning within the area which has been proven for some parts of the belt (see Sarkarinejad, 2005, 2003; Mohajjel et al., 2003; Mohajjel and Fergusson, 2000). A similar pattern can be produced within shear zones dominating by right lateral strike slip faulting (Walker and Jackson, 2004; McKenzie and Jackson, 1983) with the differential movement of the bounding faults (Bonini et al., 2003). It can be an indication of oblique converging plate boundaries with an indenter, as well (Ježek et al., 2002).

A possible explanation of such a phenomenon could be that N-S movement resulted from the plate convergence is manifested by internal rotation within the study area as a fault bounded block (Reilinger et al., 2006; Allen et al., 2004; Keilis-Borok et al., 1997). The contour plots of the stresses show a concentration of the stress along model boundaries with respect to the corresponding component. They also illustrate a relative decrease of stress values outward from the location of the applied forces i.e., the ZTL (Fig. 7). A clearly different pattern is seen for the shear component of the stress ( $S_{XY}$ ) that is somehow banded shape and nearly parallel with the ZTL (Fig. 7b). A possible reason for the variation of stress pattern across the study area could be depth dependent change of the applied velocity vector (Sarkarinejad and Barjasteh, 2008) resulting in some deflections from general rigid motion expected for simpler modeling cases (McKenzie and Jackson, 1983). The general sense of motion according to the modeled velocity field is southwest-northeast trending that initiates from south and decreases monotonically towards north till it vanishes at the northern boundary (Fig. 8). However, the local field shows rotations when approaching to the model boundaries. In the eastern boundary, a northward flow direction of the material along the Dehshir-Baft fault is predicted inside the modeled area. The velocity vectors inside the mesh are almost north-

ward trending that gradually deviated to NE and E-W along the northern boundary. The Y-component of the velocity field generally increases southwestwards supporting anti-clockwise rotation inside the modeled area. The maximum horizontal stresses are large along the eastern (DSB) boundary indicating the effect of the boundary condition (Fig. 9). The obliquity of the direction of convergence relative to the strike of the ZTL boundary is partly a reason for anti-clockwise rotation within the modeled area and partly due to the northeastward translation. The total velocity field however implies a gradual increase of shearing along the ZTL boundary.

Field data supported the modeled stress and displacement field directions (Fig. 10). A prominent trend of existing faults in E-W direction is observed in the north of the study area (Fig. 11). Few numbers of small faults with dextral strike-slip com-

ponent have also been identified (Fig. 11, right). Besides, the extensional motion along the ZTL was observed as well (Fig. 12). The northward to northeastward changing of the stress field and displacement vectors are compatible with these field data. Detailed microstructural analyses in Eghlid-Dehbid region are another support for changing in the regional stress field (Sarkarnejad and Ghanbarian, 2014; Shafei et al., 2011; Sarkarnejad and Azizi, 2008).

As the crustal thickness is a resultant of total deformation regarding to the pattern of modeled stress field (Sobouti and Arkani-Hamed, 1996), the main increase in the crust thickness is observed beneath the western ZTL boundary (Fig. 13). There is not any considerable thickening along the northern and eastern boundaries. A decrease in topography is observed from the western boundary towards the eastern boundary that

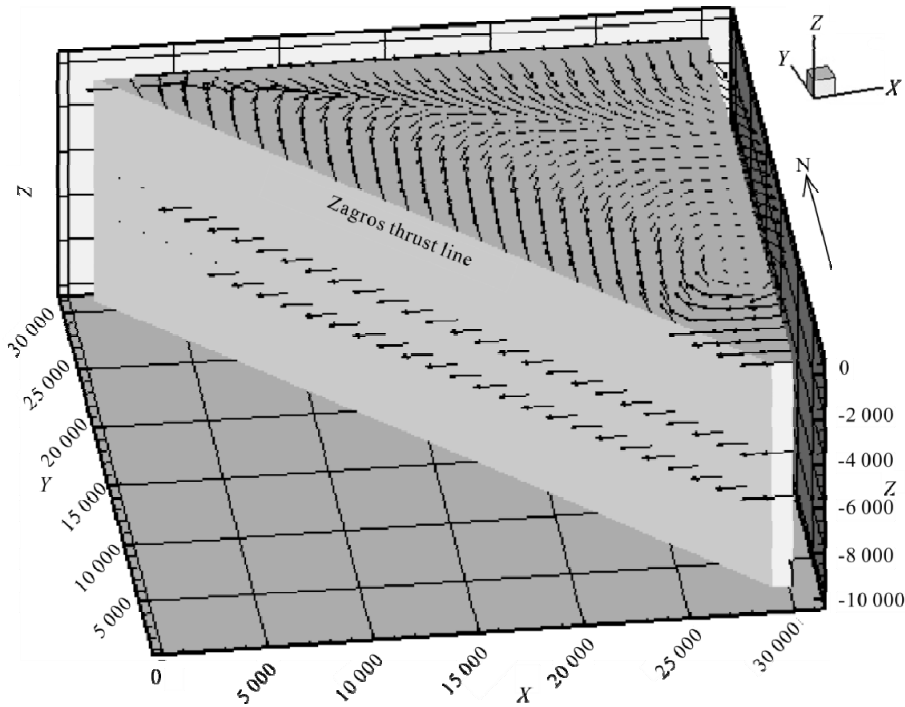


Figure 8. Plot of the modeled velocity filed for the study area.

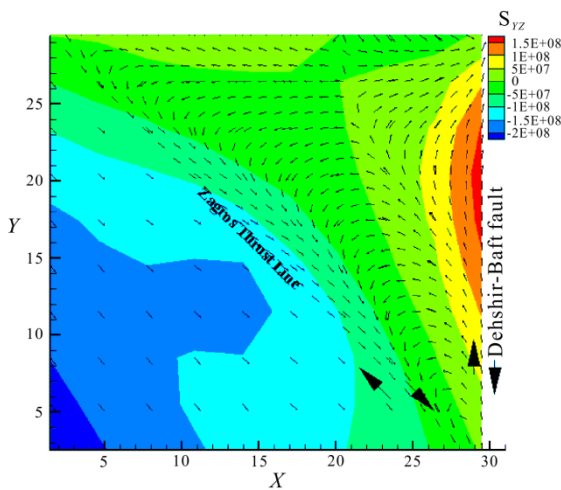


Figure 9. Two dimensional plot of the maximum horizontal stress of the modeled area.

is comparable with the existing data (Meyer et al., 2006; Arzani, 2005).

#### 4 CONCLUSIONS

The study area (Eghlid-Deh Bid) is in the northeastern part of the Zagros fold-thrust belt which is mostly inside the Sanandaj-Sirjan metamorphic belt. The modeling shows that general displacement pattern in this area is most likely from south to north which is in agreement with previous works (e.g., Bonini et al., 2003; Sobouti and Arkani-Hamed, 1996; Jackson et al., 1995) but with some rotations along the northern boundary which is partly due to the shape of the model but also coincident with some of the previous published data (Walpersdorf et al., 2006). This is affected by the E-W trend of the northern boundary that is proved by morphotectonic and GPS data. A peculiar alignment between stress field and displacement vectors along the northern boundary of the model may suggest that a basement lineament or anisotropy but more investigation is

needed. It is probable that local tectonic trends in the northern margin of the modeled region play a more significant role in deformation history. Although regional stress fields in the lithosphere are generally associated with plate driving forces but local variations of stress direction may exist at different scales

as is believed here so, local stress directions as modeled in this study are presumably associated with specific geological structures like that inferred for the upper boundary of the presented model.

The overall pattern of displacement components reveals a

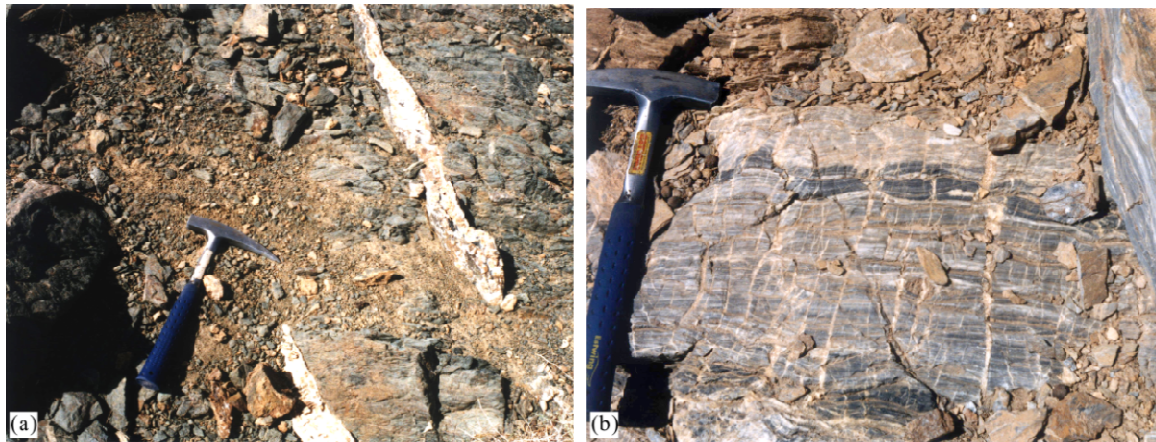


**Figure 10.** Field evidences of right lateral shear along the Zagros fault. Dextral displacement of quartz vein (a) and boudin structure (b) in the west of the study area.

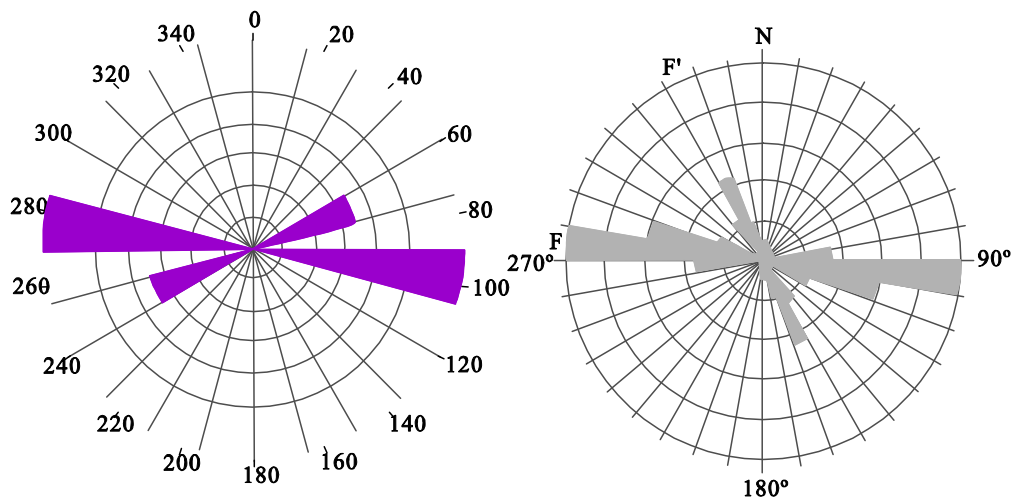


**Figure 11.** Rose diagrams of fault trends in the northeast of the study area indicating a prominent E-W alignment (left) compared to previous studies (right, modified after Arfania, 2011).

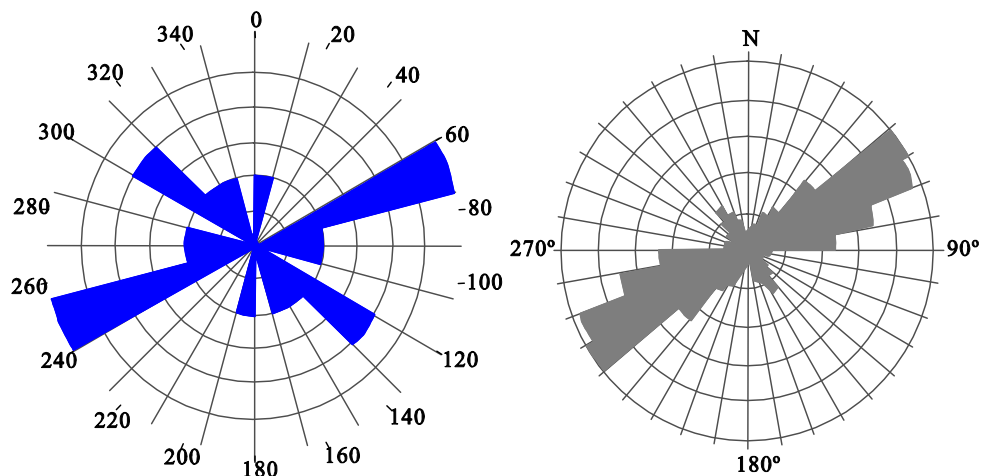


**Figure 12.** Rose diagrams of vein trends in the northeast of the study area indicating general direction of compression (left) compared to previous studies (right, modified after Arfania, 2011).

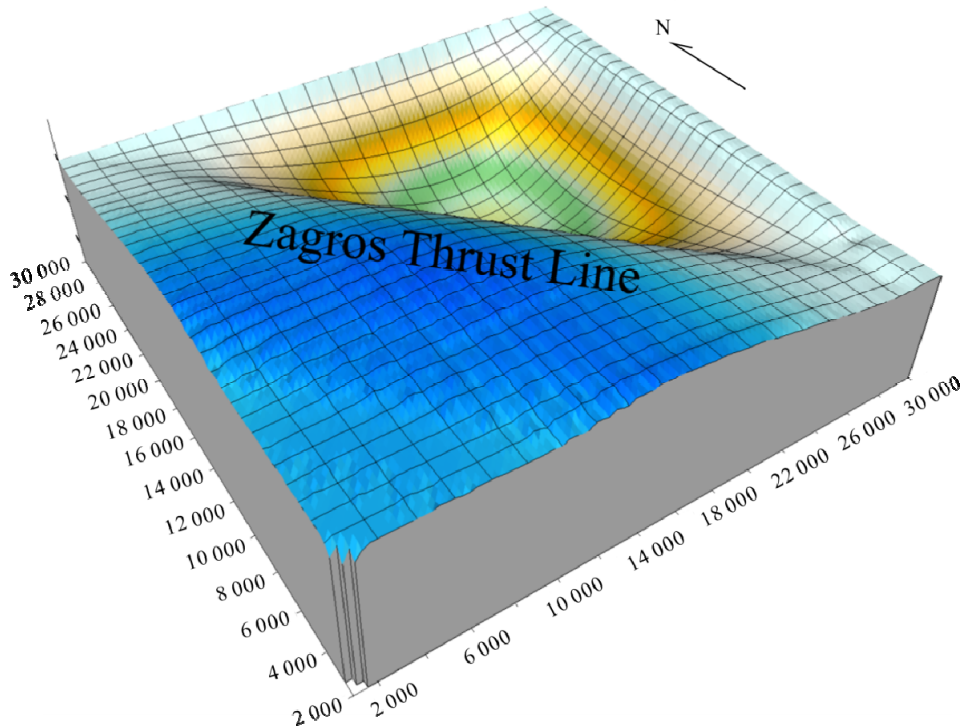


**Figure 13.** Three dimensional contour plot of crustal thickening in the study area based on the displacement data.

decrease away from the Zagros thrust line. The displacement vectors along  $Y$ -direction indicate a southward increase in its magnitude especially where the western and eastern boundaries converge. Such an increase is interpreted as a development of a component of strike-slip faulting regime that is well recorded by geomorphologic data (Meyer et al., 2006). This evidence may be used as an indicator of increasing strain rate (Vernant and Chéry, 2006b) in the region. The distribution of stress components is mainly parallel to the model boundaries regarding to the correspondent principal directions. The obtained pattern is representative for oblique converging plate boundaries and demonstrates a rotational feature which is a characteristic of shear zones with dominant right lateral strike-slip fault mechanism at its boundaries. An interesting point gained from the results is that the resulting shear stress ( $S_{XY}$ ) pattern implies an orogen-parallel distribution. Such a pattern can also indicate the activity of indentation tectonics (Ježek et al., 2002) as suggested for other parts of the belt (e.g., Kadinsky-Cade and Barazangi, 1982) but its proof is beyond the scope of this study. Additionally, the results show that the stress components are mainly concentrated at the model boundaries which are defined by major structural features such as the Zagros thrust fault, and Dehshir-Baft fault so that for the modeled area, the prevailing mechanism of shortening is mostly consistent with block structure model although the resultant patterns of stress and displacement fields are totally comparable with plate boundary shear zones.

#### ACKNOWLEDGMENTS

Most of the present study was done when the author was a Ph.D. student at Shiraz University, Iran. The author thanks Prof. K. Sarkarnejad, Department of Earth Sciences for his

supervision during his attendance at Shiraz University. The author also thanks Prof. C. Passchier who critically reviewed a very early version of the manuscript and made valuable suggestions. Two unknown reviewers gave critical and valuable comments on the manuscript that helpfully improved it and the author kindly appreciates their scientific points. Khuzestan Water & Power Authority (KWPA), Bureau of Applied Researches, is appreciated for its support. The final publication is available at Springer via <https://doi.org/10.1007/s12583-017-0682-3>.

#### REFERENCES CITED

- Allen, M., Jackson, J., Walker, R., 2004. Late Cenozoic Reorganization of the Arabia-Eurasia Collision and the Comparison of Short-Term and Long-Term Deformation Rates. *Tectonics*, 23(2): 235–273. <https://doi.org/10.1029/2003tc001530>
- Ambraseys, N. N., Jackson, J. A., 1998. Faulting Associated with Historical and Recent Earthquakes in the Eastern Mediterranean Region. *Geophysical Journal International*, 133(2): 390–406. <https://doi.org/10.1046/j.1365-246x.1998.00508.x>
- Ambraseys, N., Melville, C., 1982. *A History of Persian Earthquakes*. Cambridge University Press, Cambridge
- Arfania, R., 2011. Investigation of the Brittle and Brittle-Ductile Mesoscale Structures of the Metamorphic Area in the Southeast of Eghlid (in Persian). *Journal of Geosciences, Geological Survey of Iran*, 82: 173–180
- Arzani, N., 2005. The Fluvial Megafan of Abarkuh Basin (Central Iran): An Example of Flash-Flood Sedimentation in Arid Lands. *Geological Society, London, Special Publications*, 251(1): 41–59. <https://doi.org/10.1144/gsl.sp.2005.251.01.04>
- Berberian, F., Berberian, M., 1981. Tectono-Plutonic Episodes in Iran. In: Gupta, H. K., Delany, F. M., eds., *Zagros, Hindu Kush, Himalaya. Geodynamic Evolution*, American Geophysical Union, Geodynamics:

- Series 3. American Geophysical Union, Washington DC. 5–32
- Bird, P., 1978. Finite Element Modeling of Lithosphere Deformation: The Zagros Collision Orogeny. *Tectonophysics*, 50(2/3): 307–336. [https://doi.org/10.1016/0040-1951\(78\)90140-3](https://doi.org/10.1016/0040-1951(78)90140-3)
- Bonini, M., Corti, G., Sokoutis, D., et al., 2003. Insights from Scaled Analogue Modelling into the Seismotectonics of the Iranian Region. *Tectonophysics*, 376(3/4): 137–149. <https://doi.org/10.1016/j.tecto.2003.07.002>
- Boulin, J., 1991. Structures in Southwest Asia and Evolution of the Eastern Tethys. *Tectonophysics*, 196(3/4): 211–268. [https://doi.org/10.1016/0040-1951\(91\)90325-m](https://doi.org/10.1016/0040-1951(91)90325-m)
- DeMets, C., Gordon, R. G., Argus, D. F., et al., 1990. Current Plate Motions. *Geophysical Journal International*, 101(2): 425–478. <https://doi.org/10.1111/j.1365-246x.1990.tb06579.x>
- England, P., McKenzie, D., 1982. A Thin Viscous Sheet Model for Continental Deformation. *Geophysical Journal International*, 70(2): 295–321. <https://doi.org/10.1111/j.1365-246x.1982.tb04969.x>
- Houshmandzadeh, A. R., Ohanian, T., Sahandi, M. R., et al., 1975. Geological Map of Eghlid Quadrangle G10, 1 : 250 000. Geological Survey of Iran, Tehran, Iran
- Jackson, J., Haines, J., Holt, W., 1995. The Accommodation of Arabia-Eurasia Plate Convergence in Iran. *Journal of Geophysical Research: Solid Earth*, 100(B8): 15205–15219. <https://doi.org/10.1029/95jb01294>
- Jackson, J., McKenzie, D., 1984. Active Tectonics of the Alpine-Himalayan Belt between Western Turkey and Pakistan. *Geophysical Journal International*, 77(1): 185–264. <https://doi.org/10.1111/j.1365-246x.1984.tb01931.x>
- Ježek, J., Schulmann, K., Thompson, A. B., 2001. Strain Partitioning in Front of an Obliquely Convergent Indenter. *Stephan Mueller Special Publication Series*, 1: 93–104. doi:10.5194/smmps-1-93-2002
- Kadinsky-Cade, K., Barazangi, M., 1982. Seismotectonics of Southern Iran: The Oman Line. *Tectonics*, 1(5): 389–412. <https://doi.org/10.1029/tc001i005p00389>
- Keilis-Borok, V. I., Rotwain, I. M., Soloviev, A. A., 1997. Numerical Modeling of Block Structure Dynamics: Dependence of a Synthetic Earthquake Flow on the Structure Separateness and Boundary Movements. *J. Seismol.*, 1: 151–160
- Kreemer, C., Holt, W. E., Haines, A. J., 2003. An Integrated Global Model of Present-Day Plate Motions and Plate Boundary Deformation. *Geophysical Journal International*, 154(1): 8–34. <https://doi.org/10.1046/j.1365-246x.2003.01917.x>
- Kronberg, P., 1983. Patterns and Principles of Crustal Fracturing as Deduced from a Landsat-Mosaic Covering Central and Eastern Iran. *GSI*, 51: 37–50
- Masson, F., Chéry, J., Hatzfeld, D., et al., 2005. Seismic versus Aseismic Deformation in Iran Inferred from Earthquakes and Geodetic Data. *Geophysical Journal International*, 160(1): 217–226. <https://doi.org/10.1111/j.1365-246x.2004.02465.x>
- McKenzie, D., Jackson, J., 1983. The Relationship between Strain Rates, Crustal Thickening, Palaeomagnetism, Finite Strain and Fault Movements within a Deforming Zone. *Earth and Planetary Science Letters*, 65(1): 182–202. [https://doi.org/10.1016/0012-821x\(83\)90198-x](https://doi.org/10.1016/0012-821x(83)90198-x)
- McQuarrie, N., 2004. Crustal Scale Geometry of the Zagros Fold-Thrust Belt, Iran. *Journal of Structural Geology*, 26(3): 519–535. <https://doi.org/10.1016/j.jsg.2003.08.009>
- McQuarrie, N., Stock, J. M., Verdel, C., et al., 2003. Cenozoic Evolution of Neotethys and Implications for the Causes of Plate Motions. *Geophysical Research Letters*, 30(20): 2036. <https://doi.org/10.1029/2003gl017992>
- McQuillan, H., 1991. The Role of Basement Tectonics in the Control of Sedimentary Facies, Structural Patterns and Salt Plug Emplacements in the Zagros Fold Belt of Southwest Iran. *Journal of Southeast Asian Earth Sciences*, 5(1/2/3/4): 453–463. [https://doi.org/10.1016/0743-9547\(91\)90061-2](https://doi.org/10.1016/0743-9547(91)90061-2)
- Melosh, H. J., Raefsky, A., 1980. The Dynamical Origin of Subduction Zone Topography. *Geophysical Journal International*, 60(3): 333–354. <https://doi.org/10.1111/j.1365-246x.1980.tb04812.x>
- Melosh, H. J., Williams, C. A. Jr., 1989. Mechanics of Graben Formation in Crustal Rocks: A Finite Element Analysis. *Journal of Geophysical Research: Solid Earth*, 94(B10): 13961–13973. <https://doi.org/10.1029/jb094ib10p13961>
- Meyer, B., Mouthereau, F., Lacombe, O., et al., 2006. Evidence of Quaternary Activity along the Deshir Fault: Implication for the Tertiary Tectonics of Central Iran. *Geophysical Journal International*, 164(1): 192–201. <https://doi.org/10.1111/j.1365-246x.2005.02784.x>
- Mohajel, M., Fergusson, C. L., 2000. Dextral Transpression in Late Cretaceous Continental Collision, Sanandaj-Sirjan Zone, Western Iran. *Journal of Structural Geology*, 22(8): 1125–1139. [https://doi.org/10.1016/s0191-8141\(00\)00023-7](https://doi.org/10.1016/s0191-8141(00)00023-7)
- Mohajel, M., Fergusson, C. L., Sahandi, M. R., 2003. Cretaceous–Tertiary Convergence and Continental Collision, Sanandaj-Sirjan Zone, Western Iran. *Journal of Asian Earth Sciences*, 21(4): 397–412. [https://doi.org/10.1016/s1367-9120\(02\)00035-4](https://doi.org/10.1016/s1367-9120(02)00035-4)
- NIOC (National Iranian Oil Company), 1975. Tectonic map of South-Central Iran, Scale 1/2 500 000. Tehran
- Reilinger, R., McClusky, S., Vernant, P., et al., 2006. GPS Constraints on Continental Deformation in the Africa-Arabia-Eurasia Continental Collision Zone and Implications for the Dynamics of Plate Interactions. *Journal of Geophysical Research: Solid Earth*, 111(B5): B05411. <https://doi.org/10.1029/2005jb004051>
- Sargent, M. T., 2004. Dynamics of the Eurasian Plate: [Dissertation]. Swiss Federal Institute of Technology, Zurich. 81
- Sarkarinejad, K., 2003. Structural and Microstructural Analysis of a Palaeo-Transform Fault Zone in the Neyriz Ophiolite, Iran. *Geological Society, London, Special Publications*, 218(1): 129–145. <https://doi.org/10.1144/gsl.sp.2003.218.01.08>
- Sarkarinejad, K., 2005. Structures and Microstructures Related to Steady-State Mantle Flow in the Neyriz Ophiolite, Iran. *Journal of Asian Earth Sciences*, 25(6): 859–881. <https://doi.org/10.1016/j.jseas.2004.08.007>
- Sarkarinejad, K., Azizi, A., 2008. Slip Partitioning and Inclined Dextral Transpression along the Zagros Thrust System, Iran. *Journal of Structural Geology*, 30(1): 116–136. <https://doi.org/10.1016/j.jsg.2007.10.001>
- Sarkarinejad, K., Barjasteh, A., 2008. Modeling of Deformation Pattern in Eghlid-Deh-Bid Shear Zone of the Zagros Fold-Thrust Belt, Iran. Third International Geomodelling Conference, 22–24 Sept., 2008, Florance. 289–292
- Sarkarinejad, K., Barjasteh, A., 2010. The Role of the Zagros Suture on Three Dimensional Deformation Pattern in Eghlid-Deh Bid Area of Iran. *J. Sciences, Islamic Republic of Iran*, 21: 155–167
- Sarkarinejad, K., Ghanbarian, M. A., 2014. The Zagros Hinterland Fold-and-Thrust Belt in-Sequence Thrusting, Iran. *Journal of Asian Earth Sciences*, 85: 66–79. <https://doi.org/10.1016/j.jseas.2014.01.017>
- Seyferth, M., Henk, A., 2004. Syn-Convergent Exhumation and Lateral Extrusion in Continental Collision Zones—insights from Three-Dimensional Numerical Models. *Tectonophysics*, 382(1/2): 1–29. <https://doi.org/10.1016/j.tecto.2003.12.004>
- Shafiei, S., Alavi, S. A., Mohajel, M., 2011. Calcite Twinning Constraints on Paleostress Patterns and Tectonic Evolution of the Zagros Hinterland: The Sargaz Complex, Sanandaj-Sirjan Zone, SE Iran. *Arabian*

- Journal of Geosciences*, 4(7/8): 1189–1205.  
<https://doi.org/10.1007/s12517-010-0140-3>
- Sobouti, F., Arkani-Hamed, J., 1996. Numerical Modelling of the Deformation of the Iranian Plateau. *Geophysical Journal International*, 126(3): 805–818. <https://doi.org/10.1111/j.1365-246x.1996.tb04704.x>
- Sokoutis, D., Bonini, M., Medvedev, S., et al., 2000. Indentation of a Continent with a Built-in Thickness Change: Experiment and Nature. *Tectonophysics*, 320(3/4): 243–270. [https://doi.org/10.1016/s0040-1951\(00\)00043-3](https://doi.org/10.1016/s0040-1951(00)00043-3)
- Soofi, M. A., King, S. D., 2002. Oblique Convergence between India and Eurasia. *Journal of Geophysical Research*, 107(B5): ETG 3-1–ETG 3-8. <https://doi.org/10.1029/2001jb000636>
- Stocklin, J., 1968. Structural History and Tectonics of Iran: A Review. *AAPG Bulletin*, 52: 1229–1258. <https://doi.org/10.1306/5d25c4a5-16c1-11d7-8645000102c1865d>
- Tecplot Inc., 2005. Tecplot User's Manual Version 10. Bellevue, Washington
- Vernant, P., Chéry, J., 2006a. Mechanical Modelling of Oblique Convergence in the Zagros, Iran. *Geophysical Journal International*, 165(3): 991–1002. <https://doi.org/10.1111/j.1365-246x.2006.02900.x>
- Vernant, P., Chéry, J., 2006b. Low Fault Friction in Iran Implies Localized Deformation for the Arabia-Eurasia Collision Zone. *Earth and Planetary Science Letters*, 246(3/4): 197–206. <https://doi.org/10.1016/j.epsl.2006.04.021>
- Walker, R., Jackson, J., 2004. Active Tectonics and Late Cenozoic Strain Distribution in Central and Eastern Iran. *Tectonics*, 23(5): TC5010. <https://doi.org/10.1029/2003tc001529>
- Wallace, M. H., Melosh, H. J., 1994. Buckling of a Pervasively Faulted Lithosphere. *Pure and Applied Geophysics PAGEOPH*, 142(2): 239–261. <https://doi.org/10.1007/bf00879302>
- Walpersdorf, A., Hatzfeld, D., Nankali, H., et al., 2006. Difference in the GPS Deformation Pattern of North and Central Zagros (Iran). *Geophysical Journal International*, 167(3): 1077–1088. <https://doi.org/10.1111/j.1365-246x.2006.03147.x>